

FoX: Formation-aware exploration in multi-agent reinforcement learning

Yonghyeon Jo, Sunwoo Lee, Junghyuk Yum, Seungyul Han*

Artificial Intelligence Graduate School, UNIST, Ulsan, South Korea
{whdydgus9, c176111, yumjunhyuk, syhan}@unist.ac.kr

Abstract

Recently, deep multi-agent reinforcement learning (MARL) has gained significant popularity due to its success in various cooperative multi-agent tasks. However, exploration still remains a challenging problem in MARL due to the partial observability of the agents and the exploration space that can grow exponentially as the number of agents increases. Firstly, in order to address the scalability issue of the exploration space, we define a formation-based equivalence relation on the exploration space and aim to reduce the search space by exploring only meaningful states in different formations. Then, we propose a novel formation-aware exploration (FoX) framework that encourages partially observable agents to visit the states in diverse formations by guiding them to be well aware of their current formation solely based on their own observations. Numerical results show that the proposed FoX framework significantly outperforms the state-of-the-art MARL algorithms on Google Research Football (GRF) and sparse Starcraft II multi-agent challenge (SMAC) tasks.

1 Introduction

In recent years, multi-agent reinforcement learning (MARL) has successfully solved various real-world application challenges such as traffic control (Chu et al. 2019; Wang et al. 2019b), games (Vinyals et al. 2019), and robotic controls (Kalashnikov et al. 2018). With its increasing popularity, many multi-agent learning algorithms have been introduced (Tan 1993; Lowe et al. 2017; Rashid et al. 2018). The MARL algorithms can be broadly classified into three categories. First, the fully decentralized methods (Tan 1993; Zhang et al. 2018a) train agents independently. Second, the fully centralized methods (Gupta, Egorov, and Kochenderfer 2017) share information among agents for more efficient training. Finally, The CTDE methods (Foerster et al. 2018; Sunehag et al. 2017; Rashid et al. 2018) provide global information during training to alleviate the nonstationarity while maintaining scalability. As a result, MARL algorithms have achieved significant success in various applications.

However, MARL algorithms still face challenges from partial observability (Sukhbaatar, Szlam, and Fergus 2016).

*Corresponding author

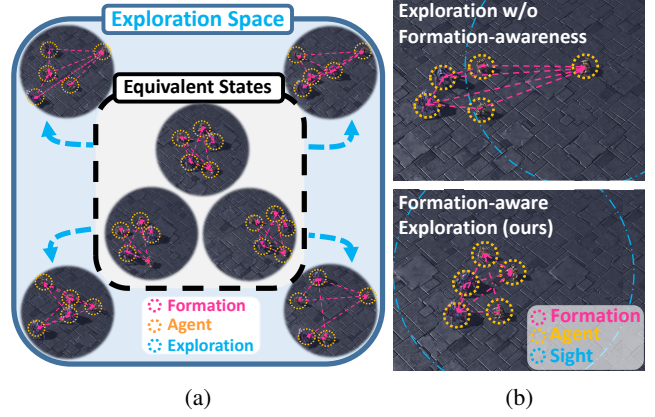


Figure 1: (a) Illustration of formation-based state equivalence. Defining state equivalence under formations can reduce the search space efficiently. (b) Illustration of formation-awareness. Our method encourages agents to be fully aware of the formation.

Even in the traditional RL, exploration is critical to prevent the agent from converging to sub-optimal policies (Ostrovski et al. 2017). To address exploration in traditional RL, exploration methods based on curiosity (Ostrovski et al. 2017; Pathak et al. 2017; Burda et al. 2019a) have been proposed. Among the curiosity explorations, count-based exploration has demonstrated simple yet efficient exploration in single-agent RL problems (Burda et al. 2019a; Tang et al. 2016). Unfortunately, the single-agent approaches may struggle in the context of MARL as partial observability makes efficient exploration even more challenging. As consideration for agent relationships exponentially increases the search space, (Wang et al. 2019a) techniques such as utilizing the influence between agents (Wang et al. 2019a) or social influence (Jaques et al. 2018) have been introduced, but despite these efforts, efficient exploration in MARL still remains a challenge (Zheng et al. 2021).

In realistic scenarios, soccer for example, it is often impractical to consider the entire information of the field upon formulating a strategy. Rather, coaches formulate strategies based on a formation, which contains the distance information between the players in soccer games. Thus, in this soccer game, formation information is critical to winning

the game against the opponents. Inspired by the real soccer game example, we define a formation in a multi-agent environment based on the differences between the agents. Based on the formation, we propose a novel formation-aware exploration (FoX) framework to visit diverse formations instead of visiting large search spaces. In FoX, we have two main contributions: 1) By defining the formation-based equivalence relation on the exploration space, we can efficiently visit states in diverse formations as illustrated in Figure 1(a), and 2) In order to overcome the partial observability of agents, we design an intrinsic reward to encourage each agent to be aware of the formation viewed by the agent as shown in Figure 1(b). In order to show the superiority of our exploration method, we conduct performance comparisons on various challenging multi-agent environments such as StarCraft II Multi-Agent Challenge (SMAC) (Samvelyan et al. 2019), and Google Research Football (GRF) (Kurach et al. 2020)

2 Related Work

Deep Multi-Agent Reinforcement Learning

With its increasing popularity, numerous MARL algorithms (Tan 1993; Foerster et al. 2016; Sunehag et al. 2017; Yang et al. 2020; Iqbal and Sha 2019; Yu et al. 2021) have been proposed. The fully decentralized methods (Tan 1993; Zhang et al. 2018b) consider agents independently during training. To address partial observability under decentralized settings, the CTDE paradigm provides global information during training. QMIX (Rashid et al. 2018) utilizes a mixing network for individual Q values of each agent to decompose the team’s expected return. QTRAN (Son et al. 2019) and QPLEX (Wang et al. 2021a) extends the value decomposition according to the principle of IGM. While the previous methods approach MARL problems with a value-based approach, (Foerster et al. 2018; Lowe et al. 2017; Wang et al. 2020b; Peng et al. 2021) address the problem via a policy-based approach.

Exploration in State Space

In environments where rewards are sparse or the state is very complex, the agent must be provided with inner motivation for efficient exploration. (Osband et al. 2016; Houthoof et al. 2016a; Nair et al. 2018; Jin et al. 2020; Machado, Bellemare, and Bowling 2020) utilizes prediction error as intrinsic rewards for exploration. (Strehl and Littman 2008; Bellemare et al. 2016; Ostrovski et al. 2017; Tang et al. 2016) designs their intrinsic rewards based on visitation count methods. While (Strehl and Littman 2008) proposes using a density model as an approximator for the number of visits to a state, (Tang et al. 2016) hashes similar states to discretize the high-dimensional state space. (Houthoof et al. 2016b; Haarnoja et al. 2018; Han and Sung 2021; Eysenbach et al. 2019) approaches exploration via information-theoretical objectives.

Intrinsic Motivations in MARL

As partial observability constraints efficient exploration in MARL, many studies have been conducted to address the

issue (Du et al. 2019; Wang et al. 2022; Gupta et al. 2021; Liu et al. 2021). Using external state information such as the agents’ location (Liu et al. 2023) can greatly assist training, but assuming such information may affect generality in the application. (Jaques et al. 2018; Wang et al. 2019a) addresses the challenge by exploring based on the influence between the agents, (Wang et al. 2020a, 2021b) assigns roles to the agents for task-appropriate behavior. (Jeon et al. 2022) targets observations with the highest sum of individual and global value as sub-goals. On the other hand, (Zheng et al. 2021) defines curiosity based on prediction errors on individual Q -values, whereas (Li et al. 2021) encourages agent diversity via local trajectory.

3 Preliminaries

Decentralized POMDP

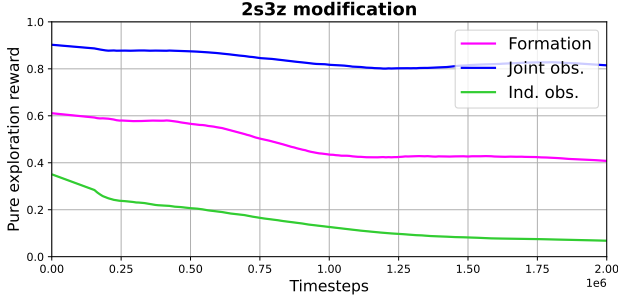
A fully cooperative multi-agent task can be seen as a decentralized partially observable Markov decision process (Dec-POMDP) (Oliehoek and Amato 2016), represented as a tuple $G = \langle \mathcal{S}, \mathcal{A}, \mathcal{P}, r, Z, O, \mathcal{O}, I, n, \gamma \rangle$. \mathcal{S} is the true state space of the environment or the observation product space of all n agents, where I is a finite set of n agents. \mathcal{A} is the set of actions. At each time step t , each agent $i \in I$ receives d -dimensional observation vector $o_t^i \in \mathcal{O}^i$ from the environment according to the observation function $O^i(s)$. Then, agents select joint action $\mathbf{a}_t = (a_t^0, \dots, a_t^{n-1})$, and the next state s_{t+1} and the global reward $r_t = R(s_t, \mathbf{a}_t)$ are generated from the environment based on the transition function $P(\cdot | s_t, \mathbf{a}_t)$ and the reward function R . Z is the latent space, and $\gamma \in [0, 1)$ is the discount factor. Each agent conditions its policy $\pi^i(a_t^i | \tau_t^i)$, where $\tau_t^i = (o_0, a_0, \dots, o_t)$ is a trajectory of i -th agent, as the agents choose their action based on their local observations. Individual policies π_i form the joint policy $\pi = \prod_{i=0}^{n-1} \pi^i$, and the main objective of RL is to maximize the cumulative reward sum $\mathbb{E}_{s_0, \mathbf{a}_0, \dots} [\sum_{t=0}^{T-1} r_t]$ given from the environment, where T is the episode length.

Centralized Training Decentralized Execution

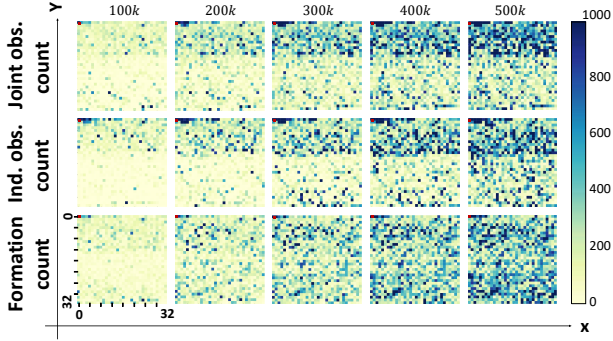
The CTDE methods provide information of the full information of agents only during training to mitigate the challenges from partial observability while maintaining decentralized execution. Among the CTDE methods are the value decomposition methods where the global value function $Q^{tot}(\boldsymbol{\tau}, \mathbf{a})$ is decomposed into individual values. A popular value decomposition method is QMIX (Rashid et al. 2018), which decomposes the global value function through a mixing network to individual agent utility functions Q^i as follows:

$$\arg\max_{\mathbf{a}} Q^{tot}(\boldsymbol{\tau}, \mathbf{a}) = \prod_{i=0}^{n-1} \arg\max_{a^i} Q^i(\tau^i, a^i), \quad (1)$$

where $\boldsymbol{\tau} = (\tau_0, \dots, \tau_{n-1})$ is the joint trajectory. Furthermore, the individual-global-max (IGM) condition must be satisfied to maintain consistency between local and global greedy actions (Son et al. 2019). The consistency between the global and local greedy actions allows greedy local actions to result in optimal global actions.



(a)



(b)

Figure 2: (a) Pure exploration reward based on visitation count graph. (b) Heatmap of diverse formation-based exploration space. With initial spawn formation at (0,0), a farther point in the heatmap indicates a larger difference in formations.

4 FoX: Formation-aware Exploration

In this section, we introduce FoX, a novel exploration framework for cooperative multi-agent reinforcement learning.

Motivation of Formation-aware Exploration

In general, the assumption of agents having information about the true global state may compromise generality. Thus, in this paper, we consider a more general scenario that agents explore the observation product space, so we define an exploration space \mathcal{S}^e as the observation product space $\mathcal{S}^e := \prod_{i \in I} \mathcal{O}^i$. Then, agents should explore diverse exploration states defined as joint observations $s_e := (o_0, \dots, o_{n-1}) \in \mathcal{S}^e$ to experience various interactions between agents well.

However, visiting all exploration states is a challenging problem since \mathcal{S}^e grows exponentially if the number of agents and the dimension of observation space increase, and it suffers from the curse of dimensionality (Bellman 1966). Thus, as motivated in real soccer games, we define the formation \mathcal{F} based on the observation differences between agents, and aim to explore diverse formations instead of the entire exploration space to reduce the search space. In order to show the importance of formation-based exploration, we conducted pure-exploration experiments in a modified 2s3z environment of SMAC (Samvelyan et al.

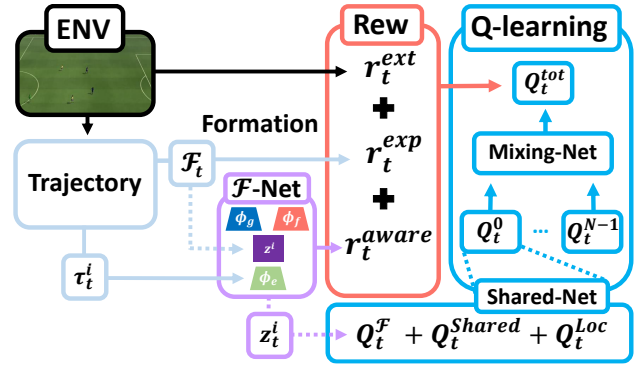


Figure 3: Schema of FoX framework

2019). In this setup, the agent only gets the pure exploration reward for count-based exploration $r_t \propto \frac{1}{\sqrt{N(s)}}$ to explore rarely visited components s . Here, we consider three types of components s for comparison: 1) joint observations (o^0, \dots, o^{n-1}) , 2) individual observations o^i , and 3) proposed formations \mathcal{F} , and details of visitation count are provided in Appendix A. Figure 2 shows the result of pure exploration, where Figure 2(a) shows the average pure exploration reward and Figure 2(b) illustrates the heatmap of the visitation frequency of diverse formations in the exploration space. In Figure 2(b), the farther point in the heatmap indicates the larger difference in formations. For the case of joint observations, the average reward does not decrease well, so most joint observations are considered novel. Thus, it only explores the limited area, as shown in Figure 2(b). For the case of individual observations, it seems that the visitation reward rapidly decreases and visits the farther area in the heatmap than the joint observation case, but it still cannot visit the diverse area in the heatmap. On the other hand, for the case of proposed formations, agents successfully visit more diverse areas in the heatmap while the pure exploration reward decreases appropriately in Figure 2(a). Thus, the pure exploration example shows that our method yields better exploration to visit diverse formations in exploration space.

Formation Arrangement

In order to reduce the search space, we aim to define a formation based on the observation differences $o^i - o^j$ between i -th agent and j -th agent, as explained in previous sections. However, The dimension of the observation difference $o^i - o^j$ is still so large that it makes exploration difficult, we first reduce the dimension of the observation difference $o_i - o_j$ as a 2-dimensional vector $D^{ij} := (\|o^i - o^j\|_2, c(o^i - o^j)) \in \mathbb{R} \times \mathbb{Z}$, where $\|\cdot\|_2$ indicates a 2-norm operator, and $c: \mathbb{R}^d \rightarrow \mathbb{Z}$ is a mapping function that transforms the angle of inputs into integers based on hash coding (Aggarwal and Verma 2015). For hash coding, SimHash (Tang et al. 2016) is used to measure the approximate angle of the observation difference, and detail of hash coding is provided in Appendix A. Then, D^{ij} contains the distance and angle information of $o^i - o^j$ in a much lower dimension.

Now, using the compressed difference D^{ij} , we define the formation $\mathcal{F}_{F^0, \dots, F^{n-1}}$ of the exploration state $s^e =$

$(o_0, \dots, o_{n-1}) \in \mathcal{S}^e$ as follows:

$$\mathcal{F}_{F^0, \dots, F^{n-1}}(s_e) = (\mathcal{F}_{F^0}^0, \dots, \mathcal{F}_{F^{n-1}}^{n-1}), \quad (2)$$

where n is the number of agents, $F^i = \{j_0, \dots, j_{k-1}\} \subset I$ is an arbitrary ordered agent index set, and $\mathcal{F}_{F^i}^i$ is the individual formation viewed by i -th agent, defined as

$$\mathcal{F}_{F^i}^i = (D^{ij_0}, \dots, D^{ij_{k-1}}). \quad (3)$$

From the definition, the formation of the exploration state s^e contains all the difference information of (i, j) agent pairs for all $i \in I, j \in F^i$. From now on, we denote the formation as \mathcal{F} for better clarity.

Finally, we can define a formation-based binary relation on the exploration state space as

$$\sim_{\mathcal{F}} := \{(s_1, s_2) \in \mathcal{S}^e \times \mathcal{S}^e \mid \mathcal{F}(s_1) = \mathcal{F}(s_2)\}, \quad (4)$$

and we can easily prove that $\sim_{\mathcal{F}}$ is an equivalence relation on the exploration space \mathcal{S}^e by Lemma 1.

Lemma 1 (Formation-based equivalence relation). *The binary relation $\sim_{\mathcal{F}}$ is an equivalence relation on the exploration space \mathcal{S}^e , i.e., two exploration states s_1 and s_2 in the exploration state \mathcal{S}^e are equivalent under $\sim_{\mathcal{F}}$ if $\mathcal{F}(s_1) = \mathcal{F}(s_2)$.*

Proof) Proof of Lemma 1 is provided in Appendix B.

Here, the dimension of formation \mathcal{F} is nk and the dimension of exploration space is nd . k depends on the selection of F^i , but in most cases, the observation dimension d is much larger than k . Thus, we can efficiently reduce the dimension of search space. In addition, based on the equivalence relation $\sim_{\mathcal{F}}$, the agents explore the exploration states in diverse formations without visiting the equivalent states that have the same formation, and it can further reduce the search space and enables better exploration as shown in Figure 2.

Formation-aware Exploration Objective

In this subsection, we propose a formation-aware exploration objective to explore states in diverse formations as

$$\underbrace{\mathcal{H}(\mathcal{F}_t)}_{(a)} + \frac{1}{n(k+1)} \sum_{i=0}^{n-1} \sum_{j \in F^{i+}} \underbrace{\mathcal{I}(\mathcal{F}_{F^i, t+1}^i; z_t^j | \tau_t^{F^{i+}}, z_t^{F^{i+} \setminus \{j\}})}_{(b)},$$

where $F^{i+} = F^i \cup \{i\}$, a^F indicates the set $\{a^i | i \in F\}$, $\mathcal{H}(X) = -p(X) \log p(X)$ is the information entropy of a random variable X , and $\mathcal{I}(X; Y) = \mathcal{H}(X) - \mathcal{H}(X|Y)$ is the mutual information between random variables X and Y .

In the exploration objective, (a) is the entropy of formations, so maximizing (a) encourages the agents to visit states in diverse formations as illustrated in Figure 1(a). Here, maximizing (a) can be accomplished by visitation count-based exploration (Ostrovski et al. 2017). We define a formation-based count exploration reward $r_t^{exp} = \frac{1}{\sqrt{N(\mathcal{F}_t)}}$, then agents get higher rewards if they visit rarely visited formations. In order to count the number of formation $N(\mathcal{F}_t)$, we use $\text{round}(\cdot)$ method to discretize the formation \mathcal{F}_t , and then count the visitation number in the discretized bins. A detailed explanation for counting is provided in Appendix A. However, agents are partially observable in MARL, so

visiting diverse formations by maximizing (a) can be a challenging problem if the agents do not know the formation information at all. Thus, we consider an additional formation-aware objective (b), which is the mutual information between the latent variable $z_t^j, \forall j \in F^{i+}$ and the next formation $\mathcal{F}_{F^i, t+1}^i$, where the trajectory τ_t^j , the trajectories $\tau_t^{F^{i+} \setminus \{j\}}$ and the latent variables $z_t^{F^{i+} \setminus \{j\}}$ of other agents are given. Then, maximizing (b) guides the i -th agent to be aware of not only its own next formation $\mathcal{F}_{F^i, t+1}^i$ but also all formations $\mathcal{F}_{F^j, t+1}^j, \forall j \text{ s.t. } i \in F^j$ to which i -th agent belongs as illustrated in Figure 1(b). Thus, we maximize both (a) and (b) to make agents visit exploration states in diverse formations while recognizing their formations well.

In order to maximize (b), we derive an evidence lower bound for the mutual information term based on the variational inference approaches (Kingma and Welling 2014; Li et al. 2021), and then we will maximize the evidence lower bound to increase the mutual information.

Lemma 2 (Evidence lower bound). *Mutual information (b) can be lower-bounded as*

$$\begin{aligned} \mathcal{I}(\mathcal{F}_{F^i, t+1}^i; z_t^j | \tau_t^{F^{i+}}, z_t^{F^{i+} \setminus \{j\}}) &\geq \\ \mathbb{E}_{\mathcal{F}_{F^i, t+1}^i, z_t^j \sim q_{\phi_e}} [\log q_{\phi_f}(\mathcal{F}_{F^i, t+1}^i | \tau_t^{F^{i+}}, z_t^{F^{i+}}) & \\ - \log p(\mathcal{F}_{F^i, t+1}^i | \tau_t^{F^{i+}}, z_t^{F^{i+} \setminus \{j\}})] & \end{aligned} \quad (5)$$

where $q_{\phi_f}(\cdot | \tau_t^{F^{i+}}, z_t^{F^{i+}})$ is an arbitrary posterior distribution, and ϕ_f and ϕ_e parameterize the distributions q_{ϕ_e} and q_{ϕ_f} , respectively.

Proof) Proof of Lemma 2 is provided in Appendix B

In the proof of Lemma 2, z_t^j is averaged over the distribution $q_{\phi_e}(\cdot | \tau_t^{F^{i+}}, z_t^{F^{i+} \setminus \{j\}})$, but it makes difficult to utilize the latent variable z_t^j in the decentralized execution setup since j -th agent cannot exploit the other agent's trajectory information. Thus, for practical implementation, we

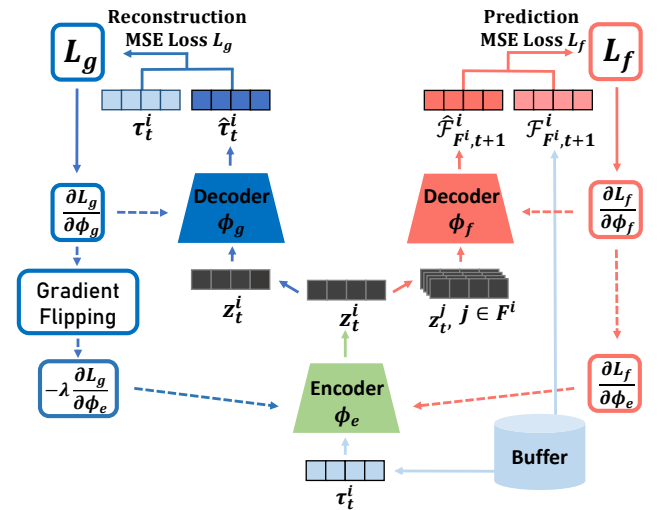


Figure 4: \mathcal{F} -Net Architecture

consider the approximate distribution $q_{\phi_e}(\cdot|\tau_t^j)$ instead of $q_{\phi_e}(\cdot|\tau_t^{F^{i+}}, z_t^{F^{i+}\setminus\{j\}})$. Then, we can formulate the encoder-decoder structure such as variational auto-encoder (VAE) (Kingma and Welling 2014), and we define an encoder $E_{\phi_e}(\tau_t^i)$ whose outputs are the mean and standard deviation of the latent variable z_t^i to sample the latent variable and a decoder $D_{\phi_f}(z_t^{F^{i+}})$ whose output is the prediction of next formation $\hat{\mathcal{F}}_{F^{i+},t+1}^i$. Here, note that we exploit the agent's trajectory τ_t^i to extract z_t^i from the encoder, but the trajectory τ_t^i may contain the redundant information regardless of the formation prediction, and it can be delivered to the latent variable z_t^i . The irrelevant information can disturb formation-aware exploration as in the case of Pathak et al. (2017). Thus, we aim to consider a gradient flipping (GF) technique proposed in the field of domain adaptation (Ganin and Lempitsky 2015) to remove the redundant information. In order to apply GF in our setup, we consider an additional trajectory decoder $D_{\phi_g}(z_t^i)$ whose output is the reconstruction of trajectory $\hat{\tau}_t^i$ and we update the encoder parameter ϕ_e to prevent the trajectory reconstruction, while decoder strives to reconstruct the trajectory. Then, we can prevent delivering useless information from the trajectory τ_t^i to the latent variable z_t^i as proposed in Ganin and Lempitsky (2015).

In summary, we can construct \mathcal{F} -Net architecture as shown in Figure 4. We define a formation prediction loss $L_f(\phi_e, \phi_f) = \frac{1}{n} \sum_{i=0}^{n-1} MSE(\mathcal{F}_{F^{i+},t+1}^i, \hat{\mathcal{F}}_{F^{i+},t+1}^i)$, a trajectory reconstruction loss $L_g(\phi_e, \phi_g) = \frac{1}{n} \sum_{i=0}^{n-1} MSE(\tau_t^i, \hat{\tau}_t^i)$, and Kullback-Leibler divergence loss $L_{KL}(\phi_e) = D_{KL}(q_{\phi_e}(\cdot|\tau_t^i) || \mathcal{N}(0, \mathbf{I}))$ as in Kingma and Welling (2014); Ganin and Lempitsky (2015), where $MSE(x, y) = \mathbb{E}[(x - y)^2]$ is the mean square error loss and $\mathcal{N}(0, \mathbf{I})$ is the multi-variate standard normal distribution with identity matrix \mathbf{I} . Based on the loss functions, we can update the encoder-decoder parameters ϕ_e, ϕ_f, ϕ_g as follows:

$$\begin{aligned} \phi_e &\leftarrow (1 - \alpha)\phi_e + \alpha \left(\frac{\partial L_f}{\partial \phi_e} + \frac{\partial L_{KL}}{\partial \phi_e} - \lambda_{GF} \frac{\partial L_g}{\partial \phi_e} \right) \\ \phi_f &\leftarrow (1 - \alpha)\phi_f + \alpha \frac{\partial L_f}{\partial \phi_f}, \quad \phi_g \leftarrow (1 - \alpha)\phi_g + \alpha \frac{\partial L_g}{\partial \phi_g}, \end{aligned} \quad (6)$$

where α is a learning rate, λ_{GF} is a hyperparameter that controls the gradient flipping effect, and we fix $\lambda_{GF} = 0.1$ in our setup. Note that ϕ_e maximizes the reconstruction loss L_g to prevent the trajectory reconstruction. Finally, in order to maximize the evidence lower bound in (5) to aware the formation information, we design the intrinsic reward r_t^{aware} that approximately represents the evidence lower bound as follows:

$$\begin{aligned} r_t^{aware} &= \frac{1}{n} \sum_{i=0}^{n-1} \left(\log q_{\phi_f}(\hat{\mathcal{F}}_{t+1}^i | \tau_t^{F^{i+}}, z_t^{F^{i+}}) \right. \\ &\quad \left. - \frac{1}{k+1} \sum_{j \in F^{i+}} \log p(\hat{\mathcal{F}}_{t+1}^i | \tau_t^{F^{i+}}, z_t^{F^{i+}\setminus\{j\}}) \right), \end{aligned} \quad (7)$$

the detailed implementation of r_t^{aware} using formation pre-

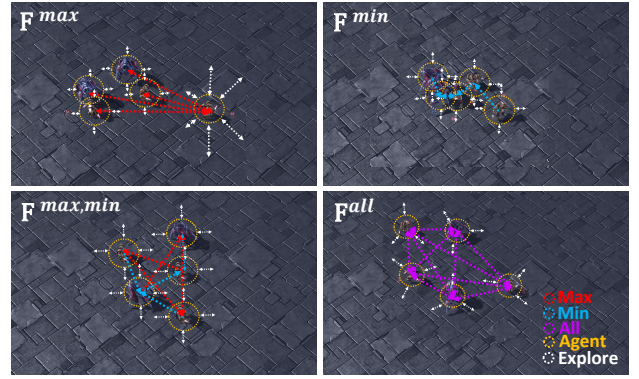


Figure 5: Formations with various agent index set F . While $F^{i,max}$, $F^{i,min}$ focuses on particular agent relationships, $F^{i,all}$ and $F^{i,max,min}$ considers extensive agent relationships.

diction loss is provided in Appendix C.

Finally, with the extrinsic reward r_t^{ext} given from the environment and intrinsic rewards r_t^{exp} and r_t^{aware} for formation-aware exploration, we can define the total reward $r_t^{tot} = r_t^{ext} + \beta_1 r_t^{exp} + \beta_2 r_t^{aware}$, where β_1 and β_2 are hyperparameters to control the effect of our intrinsic rewards r_t^{exp} and r_t^{aware} , respectively. Then, an overall temporal difference loss to update the total Q -function Q_{θ}^{tot} in (1) parameterized by θ is defined as

$$L_{TD}(\theta) = (r_t^{tot} + \gamma \max_{a'} Q_{\theta^-}^{tot}(s_{t+1}, a') - Q_{\theta}^{tot}(s_t, a_t))^2 \quad (8)$$

where θ^- is a parameter for the target network updated by the exponential moving average (EMA). We summarize the proposed FoX framework as Algorithm 1 and Figure 3.

Selection of Index Set F^i

In arranging formations, various agent index sets F^i can be considered. For example, $F^{i,max} := \{\arg\max_{j \in I \setminus \{i\}} d(i, j)\}$ forms a formation among agents with the biggest difference. In our experiments, we observe the exploration behaviors of various formations based on $F^{i,max}$, $F^{i,min} = \{\arg\min_{j \in I \setminus \{i\}} d(i, j)\}$, $F^{i,max,min} = F^{i,max} \cup F^{i,min}$, and $F^{all} = \{i | i \in I \setminus \{i\}\}$ which is illustrated in Figure 5. We conduct an ablation study for the selection of F^i , and the result shows that $F^{i,max,min}$ shows the best performance.

Formation-based Shared Network

Based on the shared network structure for individual Q -function proposed in Li et al. (2021), we aim to exploit the latent variable z_t^i . Thus, individual Q -function Q^i in (1) can be decomposed as three Q functions as follows:

$$Q^i(\tau_t^i, z_t^i, \cdot) = Q^{Shared}(\tau_t^i, \cdot) + Q^{Loc,i}(\tau_t^i, \cdot) + Q^F(z_t^i, \cdot), \quad (9)$$

where Q^{Shared} is a shared Q -function, $Q^{Loc,i}$ is i -th local Q -function, and Q^F is a Q -function that exploits formation information using z_t^i . As proposed in Li et al. (2021), we also

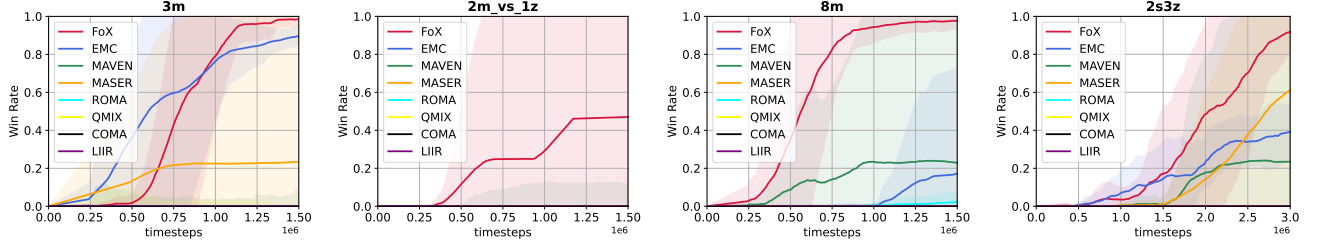


Figure 6: Performance results on SMAC(sparse)

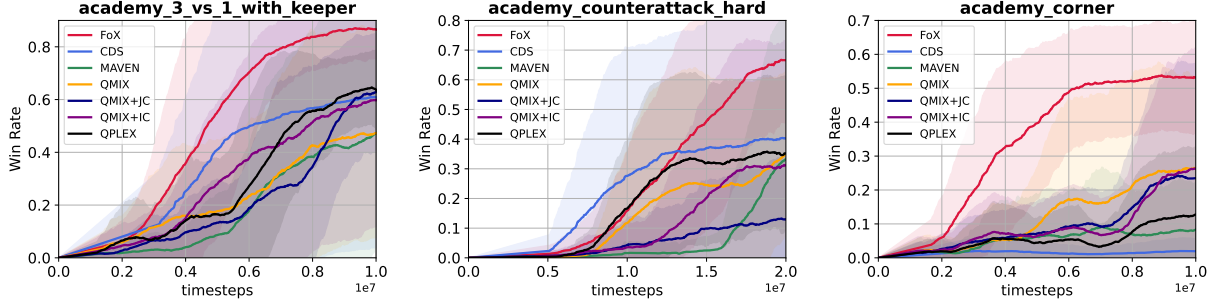


Figure 7: Performance results on GRF

Algorithm 1: FoX framework

Initialize $\phi_e, \phi_f, \phi_g, \theta, \theta^-$

- 1: **for** each epoch **do**
 - 2: **for** each gradient step **do**
 - 3: Obtain trajectory samples from environment
 - 4: Choose random batch from buffer \mathcal{D}
 - 5: Calculate formation \mathcal{F}_t from \mathbf{o}_t in (2)
 - 6: Compute intrinsic rewards r^{exp}, r^{aware}
 - 7: Compute loss functions L_f, L_g, L_{KL}, L_{TD}
 - 8: Update \mathcal{F} -Net parameters ϕ_e, ϕ_f, ϕ_g based on (6)
 - 9: Update Q -function parameter θ
 - 10: Update target parameter θ^- using EMA.
 - 11: Store samples in buffer \mathcal{D}
 - 12: **end for**
 - 13: **end for**
-

consider $l1$ regularization for $Q^{Loc,i}$ with the regularization coefficient $\lambda_{reg} = 0.1$.

5 Experiments

In our experiments, we evaluate the performance of the proposed FoX framework in the challenging cooperative multi-agent environments: the sparse StarCraft multi-agent challenge (SMAC) (Samvelyan et al. 2019) and Google Research Football (GRF) (Kurach et al. 2020). Detailed settings of the environment including the reward setting can be found in D. For hyperparameters β_1, β_2 , we have tested $\beta_1 \in \{0.001, 0.005, 0.01, 0.02, 0.1\}$ and $\beta_2 \in \{0.001, 0.005, 0.01, 0.05\}$ for both environments. Detailed hyperparameter setups can be found in Appendix E. We av-

eraged 4 seeds for SMAC tasks and 5 seeds for GRF tasks, and the solid line in the performance graph indicates the average performance, and the shaded part represents the standard deviation.

Performance on Sparse SMAC

In the original scenarios of SMAC, agents are densely rewarded for the damage they have dealt or taken in addition to sparse rewards upon the deaths of an ally or the enemy and defeating the enemy. In the sparse SMAC environment, the agents must learn with only sparse rewards without the dense rewards from the change of health point thus making the task more challenging. To leverage the fact that formation-aware exploration is not value-dependent, we conducted experiments in sparse environments. In sparse SMAC, we evaluate the performance of FoX in 4 scenarios: 3m, 8m, 2s3z, 2m_vs_1z. The exploration scheme of FoX can be easily applied to other existing MARL algorithms but as we implement FoX on QMIX during our experiments, we tested the performance of FoX against several QMIX-based algorithms including EMC (Zheng et al. 2021), MASER (Jeon et al. 2022), and ROMA (Wang et al. 2020a). Additionally, we compared FoX with MAVEN (Mahajan et al. 2019) and LIIR (Du et al. 2019) as well to compare FoX with works that address exploration. Along with COMA (Foerster et al. 2018) as a policy-gradient method. All experiments of the baselines were conducted with the author-provided codes. As both FoX and EMC can be implemented on QMIX or QPLEX (Wang et al. 2021a), we conduct our experiments with QMIX-based FoX and EMC for fair comparison. From the experimental results, we can see that in the relatively easier environment of 3m, EMC shows

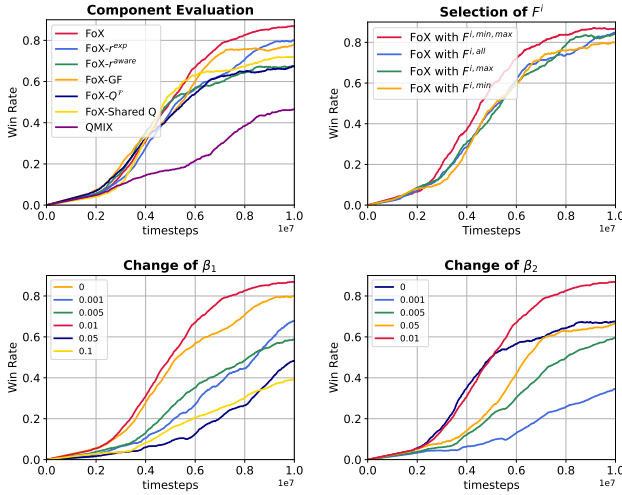


Figure 8: Ablation studies on GRF

comparable results to FoX. However, FoX significantly outperforms the other baselines in the other scenarios, where the results in 2m_vs_1z are especially notable as the other baselines struggled to learn the environment.

Performance on GRF

In Google Research Football (Kurach et al. 2020) the agents’ observation contains the location of the players, the opponents, and the ball. In our implementation, the episode is terminated and a negative reward is given to the agents when the ball goes to the other half of the court. Agents are rewarded only upon episode termination where the reward is +100 if they score else -1. In GRF, we compare the FoX framework with baselines such as QPLEX, CDS, MAVEN, and QMIX. In addition, we also compare the visitation count method implemented on QMIX, denoted as QMIX+JC for QMIX with joint observation visitation counts and QMIX+IC for the individual observation visitation counts. In our experiments, we evaluate the performance of FoX on three academy scenarios: *Academy_3_vs_1_with_keeper*, *Academy_counterattack_hard*, and *Academy_corner*. Figure 7 illustrates the performance of FoX and the baseline algorithms in the GRF scenarios. FoX shows outstanding performance in all three scenarios of the experiment, outperforming the other baselines. Especially, FoX outperforms the other visitation count baselines, supporting the idea that formation-based state equivalence efficiently reduces the search space in MARL. In addition, the exploration path of FoX agents in the GRF *Academy_counterattack_hard* can be found in Appendix F, and it shows that all agents can aware their formation well as the learning step increases.

6 Ablation Study

In this section, we analyze the individual contributions of FoX. As $\beta_1 = 0.01$ and $\beta_2 = 0.01$ showed the best performance among all GRF scenarios, we conduct our study in the GRF *Academy_3_vs_1_with_keeper* environment

with a default setting of $\beta_1 = 0.01$ and $\beta_2 = 0.01$ in our ablation studies.

Component Evaluation

To measure the effects of each component in FoX framework, we remove each component from the FoX algorithm. Component evaluation graph in Figure 8 shows the effect of various components of the intrinsic rewards r^{exp} and r^{aware} for formation-aware exploration, the gradient flipping (GF), Q -function Q^F with formation information, and shared Q learning. In Figure 8, FoX- r^{exp} and FoX- r^{aware} both show a decrease in their performance, so it shows that the intrinsic rewards are crucial components for improving the performance in FoX. Furthermore, it is noticeable that excluding Q^F and Shared Q significantly reduces the performance. Lastly, the importance of minimizing irrelevant information from individual trajectories upon latent variable extraction is shown through FoX-GF. As gradient flipping allows z to capture only the formation relevant information from τ , removing gradient flipping shows a decrease in performance.

The Effect of Intrinsic Rewards

As seen in the change of β_1 graph in Figure 8, formation-aware exploration proves its effectiveness in the *Academy_3_vs_1_with_keeper* environment since $\beta_1 = 0.01$ works better than $\beta_1 = 0$, but excessive exploration with $\beta_1 > 0.01$ can slow down the learning to explore more diverse formations. On the other hand, guiding the agents to be formation-aware helps the learning of the environment. According to the change in reward when $\beta_2 > 0.01$, the agents are guided to be aware of the formation. Being aware of the formation formulated by the other agents mitigates the information bottleneck from partial observability, boosting the learning process.

Formation Selection

According to Figure 8, formation-based on $F^{i,max}$ and $F^{i,min}$ may hold enough information to represent the agent relationship since *Academy_3_vs_1_with_keeper* presents a relatively small number of agents $n = 3$. Surprisingly, F^{all} showed a decrease in performance even though it should hold a similar amount of information to formation based on $F^{i,max,min}$. Such behavior emphasizes the importance of formation selection. To see the effect of formation selection we have to consider the environment with a large number of agents such as 2s3z as represented in Figure 5.

7 Conclusion

Exploration space which can increase exponentially upon the number of agents makes efficient exploration in MARL very challenging. In this paper, we reduce the exploration space while capturing the condensed information of the state through formations, ensuring visitation to diverse formations with awareness. Finally, the efficiency of formation-aware exploration is demonstrated in the StarCraft II Multi-Agent Challenge and Google Research FootBall, where FoX shows state-of-the-art performance.

References

- Aggarwal, K.; and Verma, H. K. 2015. Hash RC6 — Variable length Hash algorithm using RC6. In *2015 International Conference on Advances in Computer Engineering and Applications*, 450–456.
- Bellemare, M.; Srinivasan, S.; Ostrovski, G.; Schaul, T.; Saxton, D.; and Munos, R. 2016. Unifying Count-Based Exploration and Intrinsic Motivation. In Lee, D.; Sugiyama, M.; Luxburg, U.; Guyon, I.; and Garnett, R., eds., *Advances in Neural Information Processing Systems*, volume 29. Curran Associates, Inc.
- Bellman, R. 1966. Dynamic programming. *Science*, 153(3731): 34–37.
- Burda, Y.; Edwards, H.; Pathak, D.; Storkey, A.; Darrell, T.; and Efros, A. A. 2019a. Large-Scale Study of Curiosity-Driven Learning. In *International Conference on Learning Representations*.
- Burda, Y.; Edwards, H.; Storkey, A.; and Klimov, O. 2019b. Exploration by random network distillation. In *International Conference on Learning Representations*.
- Chu, T.; Wang, J.; Codecà, L.; and Li, Z. 2019. Multi-Agent Deep Reinforcement Learning for Large-Scale Traffic Signal Control. *IEEE Transactions on Intelligent Transportation Systems*, PP.
- Du, Y.; Han, L.; Fang, M.; Liu, J.; Dai, T.; and Tao, D. 2019. LIIR: Learning Individual Intrinsic Reward in Multi-Agent Reinforcement Learning. In Wallach, H.; Larochelle, H.; Beygelzimer, A.; d’Alché-Buc, F.; Fox, E.; and Garnett, R., eds., *Advances in Neural Information Processing Systems*, volume 32. Curran Associates, Inc.
- Eysenbach, B.; Gupta, A.; Ibarz, J.; and Levine, S. 2019. Diversity is All You Need: Learning Skills without a Reward Function. In *International Conference on Learning Representations*.
- Foerster, J.; Assael, I. A.; de Freitas, N.; and Whiteson, S. 2016. Learning to Communicate with Deep Multi-Agent Reinforcement Learning. In Lee, D.; Sugiyama, M.; Luxburg, U.; Guyon, I.; and Garnett, R., eds., *Advances in Neural Information Processing Systems*, volume 29. Curran Associates, Inc.
- Foerster, J. N.; Farquhar, G.; Afouras, T.; Nardelli, N.; and Whiteson, S. 2018. Counterfactual multi-agent policy gradients. In *Proceedings of the AAAI Conference on Artificial Intelligence*, volume 32.
- Ganin, Y.; and Lempitsky, V. 2015. Unsupervised domain adaptation by backpropagation. In *International conference on machine learning*, 1180–1189. PMLR.
- Gupta, J.; Egorov, M.; and Kochenderfer, M. 2017. Cooperative Multi-agent Control Using Deep Reinforcement Learning. 66–83. ISBN 978-3-319-71681-7.
- Gupta, T.; Mahajan, A.; Peng, B.; Boehmer, W.; and Whiteson, S. 2021. UneVEn: Universal Value Exploration for Multi-Agent Reinforcement Learning. In Meila, M.; and Zhang, T., eds., *Proceedings of the 38th International Conference on Machine Learning*, volume 139 of *Proceedings of Machine Learning Research*, 3930–3941. PMLR.
- Haarnoja, T.; Zhou, A.; Abbeel, P.; and Levine, S. 2018. Soft Actor-Critic: Off-Policy Maximum Entropy Deep Reinforcement Learning with a Stochastic Actor. In Dy, J.; and Krause, A., eds., *Proceedings of the 35th International Conference on Machine Learning*, volume 80 of *Proceedings of Machine Learning Research*, 1861–1870. PMLR.
- Han, S.; and Sung, Y. 2021. A Max-Min Entropy Framework for Reinforcement Learning. In Ranzato, M.; Beygelzimer, A.; Dauphin, Y.; Liang, P.; and Vaughan, J. W., eds., *Advances in Neural Information Processing Systems*, volume 34, 25732–25745. Curran Associates, Inc.
- Houthooft, R.; Chen, X.; Chen, X.; Duan, Y.; Schulman, J.; De Turck, F.; and Abbeel, P. 2016a. VIME: Variational Information Maximizing Exploration. In Lee, D.; Sugiyama, M.; Luxburg, U.; Guyon, I.; and Garnett, R., eds., *Advances in Neural Information Processing Systems*, volume 29. Curran Associates, Inc.
- Houthooft, R.; Chen, X.; Duan, Y.; Schulman, J.; De Turck, F.; and Abbeel, P. 2016b. VIME: Variational Information Maximizing Exploration.
- Iqbal, S.; and Sha, F. 2019. Actor-attention-critic for multi-agent reinforcement learning. In *International Conference on Machine Learning*, 2961–2970. PMLR.
- Jaques, N.; Lazaridou, A.; Hughes, E.; Çaglar Gülçehre; Ortega, P. A.; Strouse, D.; Leibo, J. Z.; and de Freitas, N. 2018. Social Influence as Intrinsic Motivation for Multi-Agent Deep Reinforcement Learning. In *International Conference on Machine Learning*.
- Jeon, J.; Kim, W.; Jung, W.; and Sung, Y. 2022. MASER: Multi-agent reinforcement learning with subgoals generated from experience replay buffer. In *International Conference on Machine Learning*, 10041–10052. PMLR.
- Jin, C.; Krishnamurthy, A.; Simchowitz, M.; and Yu, T. 2020. Reward-Free Exploration for Reinforcement Learning. In III, H. D.; and Singh, A., eds., *Proceedings of the 37th International Conference on Machine Learning*, volume 119 of *Proceedings of Machine Learning Research*, 4870–4879. PMLR.
- Kalashnikov, D.; Irpan, A.; Pastor, P.; Ibarz, J.; Herzog, A.; Jang, E.; Quillen, D.; Holly, E.; Kalakrishnan, M.; Vanhoucke, V.; and Levine, S. 2018. QT-Opt: Scalable Deep Reinforcement Learning for Vision-Based Robotic Manipulation.
- Kingma, D. P.; and Welling, M. 2014. Auto-Encoding Variational Bayes. In *2nd International Conference on Learning Representations, ICLR 2014, Banff, AB, Canada, April 14-16, 2014, Conference Track Proceedings*.
- Kurach, K.; Raichuk, A.; Stańczyk, P.; Zajac, M.; Bachem, O.; Espeholt, L.; Riquelme, C.; Vincent, D.; Michalski, M.; Bousquet, O.; et al. 2020. Google research football: A novel reinforcement learning environment. In *Proceedings of the AAAI conference on artificial intelligence*, volume 34, 4501–4510.
- Li, C.; Wang, T.; Wu, C.; Zhao, Q.; Yang, J.; and Zhang, C. 2021. Celebrating Diversity in Shared Multi-Agent Reinforcement Learning. In Ranzato, M.; Beygelzimer, A.; Dauphin, Y.; Liang, P.; and Vaughan, J. W., eds., *Advances in*

- Neural Information Processing Systems*, volume 34, 3991–4002. Curran Associates, Inc.
- Liu, B.; Pu, Z.; Pan, Y.; Yi, J.; Liang, Y.; and Zhang, D. 2023. Lazy Agents: A New Perspective on Solving Sparse Reward Problem in Multi-agent Reinforcement Learning. In Krause, A.; Brunskill, E.; Cho, K.; Engelhardt, B.; Sabato, S.; and Scarlett, J., eds., *Proceedings of the 40th International Conference on Machine Learning*, volume 202 of *Proceedings of Machine Learning Research*, 21937–21950. PMLR.
- Liu, I.-J.; Jain, U.; Yeh, R. A.; and Schwing, A. 2021. Co-operative Exploration for Multi-Agent Deep Reinforcement Learning. In Meila, M.; and Zhang, T., eds., *Proceedings of the 38th International Conference on Machine Learning*, volume 139 of *Proceedings of Machine Learning Research*, 6826–6836. PMLR.
- Lowe, R.; Wu, Y.; Tamar, A.; Harb, J.; Abbeel, P.; and Mordatch, I. 2017. Multi-Agent Actor-Critic for Mixed Cooperative-Competitive Environments. In *NIPS*.
- Machado, M.; Bellemare, M.; and Bowling, M. 2020. Count-Based Exploration with the Successor Representation. *Proceedings of the AAAI Conference on Artificial Intelligence*, 34: 5125–5133.
- Mahajan, A.; Rashid, T.; Samvelyan, M.; and Whiteson, S. 2019. MAVEN: Multi-agent variational exploration. *Advances in Neural Information Processing Systems*, 32.
- Nair, A.; McGrew, B.; Andrychowicz, M.; Zaremba, W.; and Abbeel, P. 2018. Overcoming Exploration in Reinforcement Learning with Demonstrations. In *2018 IEEE International Conference on Robotics and Automation (ICRA)*, 6292–6299.
- Oliehoek, F. A.; and Amato, C. 2016. *A Concise Introduction to Decentralized POMDPs*. Springer Publishing Company, Incorporated, 1st edition. ISBN 3319289276.
- Osband, I.; Blundell, C.; Pritzel, A.; and Van Roy, B. 2016. Deep Exploration via Bootstrapped DQN. In Lee, D.; Sugiyama, M.; Luxburg, U.; Guyon, I.; and Garnett, R., eds., *Advances in Neural Information Processing Systems*, volume 29. Curran Associates, Inc.
- Ostrovski, G.; Bellemare, M.; Oord, A.; and Munos, R. 2017. Count-Based Exploration with Neural Density Models.
- Pathak, D.; Agrawal, P.; Efros, A. A.; and Darrell, T. 2017. Curiosity-driven Exploration by Self-supervised Prediction. In Precup, D.; and Teh, Y. W., eds., *Proceedings of the 34th International Conference on Machine Learning*, volume 70 of *Proceedings of Machine Learning Research*, 2778–2787. PMLR.
- Peng, B.; Rashid, T.; Schroeder de Witt, C.; Kamienny, P.-A.; Torr, P.; Böhm, W.; and Whiteson, S. 2021. FAC-MAC: Factored multi-agent centralised policy gradients. *Advances in Neural Information Processing Systems*, 34: 12208–12221.
- Rashid, T.; Samvelyan, M.; Schroeder, C.; Farquhar, G.; Forster, J.; and Whiteson, S. 2018. QMIX: Monotonic value function factorisation for deep multi-agent reinforcement learning. In *International Conference on Machine Learning*, 4295–4304. PMLR.
- Samvelyan, M.; Rashid, T.; De Witt, C. S.; Farquhar, G.; Nardelli, N.; Rudner, T. G.; Hung, C.-M.; Torr, P. H.; Forster, J.; and Whiteson, S. 2019. The starcraft multi-agent challenge. *arXiv preprint arXiv:1902.04043*.
- Senavirathne, N.; and Torra, V. 2019. Rounding based continuous data discretization for statistical disclosure control. *Journal of Ambient Intelligence and Humanized Computing*.
- Son, K.; Kim, D.; Kang, W. J.; Hostallero, D. E.; and Yi, Y. 2019. QTRAN: Learning to factorize with transformation for cooperative multi-agent reinforcement learning. In *International Conference on Machine Learning*, 5887–5896. PMLR.
- Strehl, A.; and Littman, M. 2008. An Analysis of Model-Based Interval Estimation for Markov Decision Processes. *Journal of Computer and System Sciences*, 74: 1309–1331.
- Sukhbaatar, S.; Szlam, A.; and Fergus, R. 2016. Learning Multiagent Communication with Backpropagation.
- Sunehag, P.; Lever, G.; Gruslys, A.; Czarnecki, W. M.; Zambaldi, V.; Jaderberg, M.; Lanctot, M.; Sonnerat, N.; Leibo, J. Z.; Tuyls, K.; et al. 2017. Value-decomposition networks for cooperative multi-agent learning. *arXiv preprint arXiv:1706.05296*.
- Tan, M. 1993. Multi-agent reinforcement learning: Independent vs. cooperative agents. In *Proceedings of the Tenth International Conference on Machine Learning*, 330–337.
- Tang, H.; Houthoofd, R.; Foote, D.; Stooke, A.; Chen, X.; Duan, Y.; Schulman, J.; De Turk, F.; and Abbeel, P. 2016. #Exploration: A Study of Count-Based Exploration for Deep Reinforcement Learning.
- Vinyals, O.; Babuschkin, I.; Czarnecki, W.; Mathieu, M.; Dudzik, A.; Chung, J.; Choi, D.; Powell, R.; Ewalds, T.; Georgiev, P.; Oh, J.; Horgan, D.; Kroiss, M.; Danihelka, I.; Huang, A.; Sifre, L.; Cai, T.; Agapiou, J.; Jaderberg, M.; and Silver, D. 2019. Grandmaster level in StarCraft II using multi-agent reinforcement learning. *Nature*, 575.
- Wang, J.; Ren, Z.; Liu, T.; Yu, Y.; and Zhang, C. 2021a. {QPLEX}: Duplex Dueling Multi-Agent Q-Learning. In *International Conference on Learning Representations*.
- Wang, L.; Zhang, Y.; Hu, Y.; Wang, W.; Zhang, C.; Gao, Y.; Hao, J.; Lv, T.; and Fan, C. 2022. Individual Reward Assisted Multi-Agent Reinforcement Learning. In Chaudhuri, K.; Jegelka, S.; Song, L.; Szepesvari, C.; Niu, G.; and Sabato, S., eds., *Proceedings of the 39th International Conference on Machine Learning*, volume 162 of *Proceedings of Machine Learning Research*, 23417–23432. PMLR.
- Wang, T.; Dong, H.; Lesser, V.; and Zhang, C. 2020a. ROMA: Multi-agent reinforcement learning with emergent roles. *arXiv preprint arXiv:2003.08039*.
- Wang, T.; Gupta, T.; Mahajan, A.; Peng, B.; Whiteson, S.; and Zhang, C. 2021b. {RODE}: Learning Roles to Decompose Multi-Agent Tasks. In *International Conference on Learning Representations*.
- Wang, T.; Wang, J.; Wu, Y.; and Zhang, C. 2019a. Influence-Based Multi-Agent Exploration. *ArXiv*, abs/1910.05512.
- Wang, X.; Ke, L.; Qiao, Z.; and Chai, X. 2019b. Large-scale Traffic Signal Control Using a Novel Multi-Agent Reinforcement Learning.

Wang, Y.; Han, B.; Wang, T.; Dong, H.; and Zhang, C. 2020b. DOP: Off-policy multi-agent decomposed policy gradients. In *International Conference on Learning Representations*.

Yang, Y.; Hao, J.; Liao, B.; Shao, K.; Guangyong, C.; Liu, W.; and Tang, H. 2020. Qatten: A General Framework for Cooperative Multiagent Reinforcement Learning. *arXiv preprint arXiv:2002.03939*.

Yu, C.; Velu, A.; Vinitsky, E.; Wang, Y.; Bayen, A.; and Wu, Y. 2021. The surprising effectiveness of ppo in cooperative, multi-agent games. *arXiv preprint arXiv:2103.01955*.

Zhang, K.; Yang, Z.; Liu, H.; Zhang, T.; and Basar, T. 2018a. Fully Decentralized Multi-Agent Reinforcement Learning with Networked Agents. In Dy, J.; and Krause, A., eds., *Proceedings of the 35th International Conference on Machine Learning*, volume 80 of *Proceedings of Machine Learning Research*, 5872–5881. PMLR.

Zhang, K.; Yang, Z.; Liu, H.; Zhang, T.; and Basar, T. 2018b. Fully Decentralized Multi-Agent Reinforcement Learning with Networked Agents. In Dy, J.; and Krause, A., eds., *Proceedings of the 35th International Conference on Machine Learning*, volume 80 of *Proceedings of Machine Learning Research*, 5872–5881. PMLR.

Zheng, L.; Chen, J.; Wang, J.; He, J.; Hu, Y.; Chen, Y.; Fan, C.; Gao, Y.; and Zhang, C. 2021. Episodic Multi-agent Reinforcement Learning with Curiosity-driven Exploration. In Ranzato, M.; Beygelzimer, A.; Dauphin, Y.; Liang, P.; and Vaughan, J. W., eds., *Advances in Neural Information Processing Systems*, volume 34, 3757–3769. Curran Associates, Inc.

A Detailed Explanation for Discretization Methods

A.1 Discretization for D^{ij}

In defining formation \mathcal{F} , we calculate the difference between the observation of the agents in order to reduce the search space. As explained in Section 4 of the proposed paper, using $o^i - o^j$ still yields a search space of high dimension, so we propose to reduce the dimension of the observation difference $o_i - o_j$ as a 2-dimensional vector $D^{ij} := (\|o^i - o^j\|_2, c(o^i - o^j)) \in \mathbb{R} \times \mathbb{Z}$, where $\|\cdot\|_2$ indicates a 2-norm operator, and a mapping function $c : \mathbb{R}^d \rightarrow \mathbb{Z}$ in D^{ij} discretizes the angle between the agent observations $\frac{o^i - o^j}{\|o^i - o^j\|_2}$ as an integer number based on hash coding (Aggarwal and Verma 2015) as follows:

1) First, we transform $\frac{o^i - o^j}{\|o^i - o^j\|_2}$ into a hash code h based on SimHash (Tang et al. 2016). Here, we use SimHash (Tang et al. 2016) for hash coding since it is popularly considered for hash coding. In SimHash, we generate a random vector $v = \mathbb{R}^{m \times d}$ where m is the parameter for the length of the hash code and d is the input dimension, and a hash code $h = \text{sign}(v \cdot \frac{o^i - o^j}{\|o^i - o^j\|_2})$,

where the sign function $\text{sign}(\cdot)$ is defined as $\text{sign}(x) = \begin{cases} 1, & \text{if } x \geq 0 \\ 0, & \text{if } x < 0 \end{cases}$.

2) Then, the resulting binary vector h of length m is transformed into an integer number $c(o_i - o_j) = h_{int} \in \{0, \dots, 2^m - 1\}$, discretizing the angle between the observation difference $o^i - o^j$ into 2^m categories. In our experiments, we set $m = 9$ since c represents the angle of the observation difference as 512 ways well enough.

A.2 Discretization for visitation count

In visitation count, we consider the discretization based on a round function $\text{round}(\cdot)$ for visitation count to discretize the input more accurately than SimHash. In Python, $\text{round}(\cdot)$ returns the input value rounded to l -th decimal places as follows:

$$\text{round}(x) = \begin{cases} \text{floor}(x \cdot 10^l) \cdot 10^{-l}, & \text{if } x \cdot 10^l - \text{floor}(x \cdot 10^l) < 0.5 \\ (\text{floor}(x \cdot 10^l) + 1) \cdot 10^{-l}, & \text{otherwise} \end{cases}.$$

While performing $\text{round}()$ with too small l causes all input data to be binned together, using a very high value of l distinguishes all inputs differently (Senavirathne and Torra 2019). Therefore, setting an appropriate l value is important in visitation count methods. In our setup, $l = 1$ or 3 works well for SMAC and GRF environments. Then, we count the number of visitation $N(s)$ based on the output of $\text{round}(\cdot)$ function, where s can be any component such as joint observations (o^0, \dots, o^{n-1}) , individual observations o^j , and our proposed formation \mathcal{F} . Then, we can setup the pure exploration reward $r^{exp} \propto \frac{1}{\sqrt{N(s)}}$ to explore rarely visited components.

B Proofs

B.1 Proof of Lemma 1

Lemma 1 (Formation-based equivalence relation) *The binary relation $\sim_{\mathcal{F}}$ is an equivalence relation on the exploration space \mathcal{S}^e , i.e., two exploration states s_1 and s_2 in the exploration state \mathcal{S}^e are equivalent under $\sim_{\mathcal{F}}$ if $\mathcal{F}(s_1) = \mathcal{F}(s_2)$.*

Proof To prove Lemma 1, we have to show that $\sim_{\mathcal{F}}$ satisfies 3 properties of equivalence relation: $s_1 \sim_{\mathcal{F}} s_1$ (reflexivity) from the definition, if $s_1 \sim_{\mathcal{F}} s_2$ then $s_1 \sim_{\mathcal{F}} s_2$ (symmetry), and if $s_1 \sim_{\mathcal{F}} s_2$ and $s_2 \sim_{\mathcal{F}} s_3$, then $s_1 \sim_{\mathcal{F}} s_3$ (transitivity), $\forall s_1, s_2, s_3 \in \mathcal{S}^e$.

1) Reflexivity: For all $s_1 \in \mathcal{S}^e$, $\mathcal{F}(s_1) = \mathcal{F}(s_1)$, showing $s_1 \sim_{\mathcal{F}} s_1$

2) Symmetry: For all $s_1, s_2 \in \mathcal{S}^e$ such that $s_1 \sim_{\mathcal{F}} s_2$, $\mathcal{F}(s_1) = \mathcal{F}(s_2)$ implying $\mathcal{F}(s_2) = \mathcal{F}(s_1)$. Therefore, $s_2 \sim_{\mathcal{F}} s_1$.

3) Transitivity: Suppose $\forall s_1, s_2, s_3 \in \mathcal{S}^e$ such that $s_1 \sim_{\mathcal{F}} s_2$ and $s_2 \sim_{\mathcal{F}} s_3$. As $\mathcal{F}(s_1) = \mathcal{F}(s_2)$ and $\mathcal{F}(s_2) = \mathcal{F}(s_3)$ from the definition of $\sim_{\mathcal{F}}$, we have $\mathcal{F}(s_1) = \mathcal{F}(s_3)$, indicating $s_1 \sim_{\mathcal{F}} s_3$.

Thus, $\sim_{\mathcal{F}}$ is an equivalence relation on \mathcal{S}^e .

B.2 Proof of Lemma 2

Lemma 2 (Evidence lower bound) *Mutual information (b) can be lower-bounded as*

$$\mathcal{I}(\mathcal{F}_{F^i, t+1}^i; z_t^j | \tau_t^{F^{i+}}, z_t^{F^{i+} \setminus \{j\}}) \geq \mathbb{E}_{\mathcal{F}_{F^i, t+1}^i, z_t^j \sim q_{\phi_e}} [\log q_{\phi_f}(\mathcal{F}_{F^i, t+1}^i | \tau_t^{F^{i+}}, z_t^{F^{i+}}) - \log p(\mathcal{F}_{F^i, t+1}^i | \tau_t^{F^{i+}}, z_t^{F^{i+} \setminus \{j\}})], \quad (10)$$

Proof

$$\begin{aligned} & \mathcal{I}(\mathcal{F}_{F^i, t+1}^i; z_t^j | \tau_t^{F^{i+}}, z_t^{F^{i+} \setminus \{j\}}) \\ &= \sum_{\mathcal{F}_{F^i, t+1}^i} \sum_{z_t^j} p(\mathcal{F}_{F^i, t+1}^i | \tau_t^{F^{i+}}, z_t^{F^{i+} \setminus \{j\}}) \left\{ \log p(\mathcal{F}_{F^i, t+1}^i | \tau_t^{F^{i+}}, z_t^{F^{i+}}) - \log p(\mathcal{F}_{F^i, t+1}^i | \tau_t^{F^{i+}}, z_t^{F^{i+} \setminus \{j\}}) \right\} \\ &= \sum_{\mathcal{F}_{F^i, t+1}^i} \sum_{z_t^j} p(\mathcal{F}_{F^i, t+1}^i | \tau_t^{F^{i+}}, z_t^{F^{i+} \setminus \{j\}}) q_{\phi_e}(z_t^j | \tau_t^{F^{i+}}, z_t^{F^{i+} \setminus \{j\}}) \left\{ \log p(\mathcal{F}_{F^i, t+1}^i | \tau_t^{F^{i+}}, z_t^{F^{i+}}) \right. \\ &\quad \left. - \log p(\mathcal{F}_{F^i, t+1}^i | \tau_t^{F^{i+}}, z_t^{F^{i+} \setminus \{j\}}) \right\} \\ &= \sum_{\mathcal{F}_{F^i, t+1}^i} \sum_{z_t^j} p(\mathcal{F}_{F^i, t+1}^i | \tau_t^{F^{i+}}, z_t^{F^{i+} \setminus \{j\}}) q_{\phi_e}(z_t^j | \tau_t^{F^{i+}}, z_t^{F^{i+} \setminus \{j\}}) \left\{ \log p(\mathcal{F}_{F^i, t+1}^i | \tau_t^{F^{i+}}, z_t^{F^{i+}}) \right. \\ &\quad \left. - \log q_{\phi_f}(\mathcal{F}_{F^i, t+1}^i | \tau_t^{F^{i+}}, z_t^{F^{i+}}) + \log q_{\phi_f}(\mathcal{F}_{F^i, t+1}^i | \tau_t^{F^{i+}}, z_t^{F^{i+}}) - \log p(\mathcal{F}_{F^i, t+1}^i | \tau_t^{F^{i+}}, z_t^{F^{i+} \setminus \{j\}}) \right\} \\ &= \sum_{z_t^j} q_{\phi_e}(z_t^j | \tau_t^{F^{i+}}, z_t^{F^{i+} \setminus \{j\}}) \cdot \underbrace{\sum_{\mathcal{F}_{F^i, t+1}^i} p(\mathcal{F}_{F^i, t+1}^i | \tau_t^{F^{i+}}, z_t^{F^{i+}}) \log \frac{p(\mathcal{F}_{F^i, t+1}^i | \tau_t^{F^{i+}}, z_t^{F^{i+}})}{q(\mathcal{F}_{F^i, t+1}^i | \tau_t^{F^{i+}}, z_t^{F^{i+}})}}_{D_{KL}(p(\cdot | \tau_t^{F^{i+}}, z_t^{F^{i+}}) || q(\cdot | \tau_t^{F^{i+}}, z_t^{F^{i+}})) \geq 0} \\ &\quad + \sum_{\mathcal{F}_{F^i, t+1}^i} \sum_{z_t^j} p(\mathcal{F}_{F^i, t+1}^i | \tau_t^{F^{i+}}, z_t^{F^{i+} \setminus \{j\}}) q_{\phi_e}(z_t^j | \tau_t^{F^{i+}}, z_t^{F^{i+} \setminus \{j\}}) \left\{ \log q_{\phi_f}(\mathcal{F}_{F^i, t+1}^i | \tau_t^{F^{i+}}, z_t^{F^{i+}}) - \log p(\mathcal{F}_{F^i, t+1}^i | \tau_t^{F^{i+}}, z_t^{F^{i+}}) \right\} \\ &\geq \sum_{\mathcal{F}_{F^i, t+1}^i} \sum_{z_t^j} p(\mathcal{F}_{F^i, t+1}^i | \tau_t^{F^{i+}}, z_t^{F^{i+} \setminus \{j\}}) q_{\phi_e}(z_t^j | \tau_t^{F^{i+}}, z_t^{F^{i+} \setminus \{j\}}) \left\{ \log q_{\phi_f}(\mathcal{F}_{F^i, t+1}^i | \tau_t^{F^{i+}}, z_t^{F^{i+}}) - \log p(\mathcal{F}_{F^i, t+1}^i | \tau_t^{F^{i+}}, z_t^{F^{i+}}) \right\} \\ &= \mathbb{E}_{\mathcal{F}_{F^i, t+1}^i, z_t^j \sim q_{\phi_e}} [\log q_{\phi_f}(\mathcal{F}_{F^i, t+1}^i | \tau_t^{F^{i+}}, z_t^{F^{i+}}) - \log p(\mathcal{F}_{F^i, t+1}^i | \tau_t^{F^{i+}}, z_t^{F^{i+} \setminus \{j\}})], \end{aligned} \quad (11)$$

which concludes the proof.

C Approximation of Posterior Distributions

Since q_{ϕ_f} is an arbitrary posterior distribution in Lemma 2, so for implementation of r^{aware} , we set the posterior distribution $\log q_{\phi_f}$ in the evidence lower bound term as the prediction error of next formation, i.e., $\log q_{\phi_f}(\hat{\mathcal{F}}_{t+1}^i | \tau_t^{F^{i+}}, z_t^{F^{i+}}) \approx -MSE(\mathcal{F}_{F^i, t+1}^i, \hat{\mathcal{F}}_{F^i, t+1}^i)$. Also, we approximate the latter term $\log p$ using the prediction error as $\log p(\hat{\mathcal{F}}_{t+1}^i | \tau_t^{F^{i+}}, z_t^{F^{i+} \setminus \{j\}}) \approx \log \mathbb{E}_{z_j \sim q_e} [q_{\phi_f}(\hat{\mathcal{F}}_{t+1}^i | \tau_t^{F^{i+}}, z_t^{F^{i+} \setminus \{j\}})] \approx \log \mathbb{E}_{z_j \sim q_e} [\exp(-MSE(\mathcal{F}_{F^i, t+1}^i, \hat{\mathcal{F}}_{F^i, t+1}^i))]$. However, in this paper, we just use more simple approximation $\log p \approx \mathbb{E}_{z^j \sim \mathcal{N}(0, \mathbf{I})} [-MSE(\mathcal{F}_{F^i, t+1}^i, \hat{\mathcal{F}}_{F^i, t+1}^i)]$ for practical implementation under the assumption that q_{ϕ_e} is close enough to $\mathcal{N}(0, \mathbf{I})$ by reducing L_{KL} .

D Detailed Environment Description

Our implementations are based on the open-source code from Samvelyan et al. (2019) in PyTorch. For computational resources, we used NVIDIA RTX 3090 GPU, Intel Xeon Gold 6348 CPU On Ubuntu 20.04. The training for SMAC scenarios can be done in less than one day, whereas training on the scenarios from GRF can be done in less than two days per 5,000,000 time steps.

D.1 StarCraft Multi-Agent Challenge

The StarCraft Multi-Agent Challenge is an environment where two teams composed of StarCraft units engage in combat to maximize win rates. This stands as a prominent benchmark for evaluating multi-agent systems because it requires units

to cooperate with each other. In this setting, the enemy team consists of units controlled by the built-in game AI, which utilizes predefined non-learned heuristics. An army team comprises individual units treated as separate agents and trained using reinforcement learning(ai) algorithms.

Units possess local observations, primarily within their field of sight. The observation vector includes distances, relative x, relative y, health, shield, and unit types of both allied and enemy units within their visual range. Additionally, a global state for centralized learning contains information on all units on the map, including coordinates, local observations, energy of Medivacs, cooldowns of allied units, and the last actions of all agents. Agents operate within a discrete action space consisting of move[direction], attack [enemy_id], stop, and no-op. Rewards in SMAC come in two main settings, dense rewards, and sparse rewards. Dense rewards include rewards for hit-point damage dealt, enemy units killed, and winning the battle. Sparse rewards consist of a reward of +1 for winning and -1 for losing an episode. Moreover, ‘Partially sparse rewards’ provide rewards when killing an opponent’s unit, losing one of our units, or winning a battle. This is the primary reward setting we intend to use.

Event	Dense reward	Sparse reward
Death of single enemy	+10	+10
Death of single ally	-5	-5
Win	+200	+200
Enemy hit-point	-Enemy hit-point	-
Ally hit-point	+Ally hit-point	-
Other elements	+/- elements such as ‘shield’	-

Table 1: The reward setting for dense and sparse SMAC environment.

SMAC consists of various micromanagement scenarios designed to evaluate the effectiveness of multi-agent learning in solving challenging tasks that require coordinated action. Each scenario defines initial positions, numbers, and types of units. An episode concludes when all units are defeated or after a specified episode length. For our experiments, we use the 2m_vs_1z, 3m, 8m, and 2s3z scenarios. In SMAC Sparse, when agents are given positive rewards beyond those provided by the environment, agents tend to focus on prolonging the episode instead of defeating the enemy units, falling into local optima. Hence, in the case of SMAC Sparse, we normalized our intrinsic rewards r^{exp} and r^{aware} to be less than or equal to zero. As agents are penalized upon needlessly prolonging the episode, our intrinsic rewards prevent the agents from falling into local optima. A similar approach has been proposed in previous works with comparable sparse reward settings, such as Jeon et al. (2022).

D.2 Google Research Football

Google Research Football implements the common aspects of football such as goals, fouls, corners, penalty kicks, and offsides. The opposing team consists of rule-based AI bots in the original GameplayFootball. The bot’s reaction time and decision-making speed can be adjustable. The state is defined by ball position, possession, coordinates of players, active player, and game state. Observations are offered in three representations: pixels, super mini-map (SMM), and float. The pixel representation is a 1280x720 RGB image containing information like the scoreboard and small map, enabling the provision of all player positions. The super mini-map is a 72x96 matrix encoding the home team, away team, ball, and active player for the current time step. The floats representation consists of a 115-dimensional encoded vector for players’ coordinates, ball possession and direction, and the active player’s game mode. we use the floats method.

Action space consists of 8-directional standard move actions, various ways to kick the ball, sprint, slide tackle, and dribble. Rewards consist of two functions: scoring and checkpoint rewards. Scoring rewards are +1 when our team scores a goal and -1 if the opposing team scores. Checkpoint rewards divide the area around the opposing goal into 10 checkpoints based on Euclidean distance. When scoring from a checkpoint, agents receive a +0.1 reward, reaching a maximum of +1 reward. In our experiments, the agents are rewarded based on scoring rewards. Additionally, to expedite the iterations of the learning process, there’s a football academy with 11 simpler scenarios, each emulating specific situations that can occur in actual soccer matches. Episodes can conclude when the ball is lost, or our team scores a goal before reaching the limit. In our experiments, we use the *Academy_3_vs_1_with_keeper*, *Academy_counterattack_hard*, and *Academy_corner* environments. Upon using prediction error as a measure for exploration bonus, the scale of the observation can greatly affect the consistency of the reward scale (Burda et al. 2019b). Therefore in GRF, we normalized r^{aware} to scale progressively with the prediction error.

E Hyperparameter Setup

In this section, we discuss the hyperparameters used in our experiments. As we compare the performance of FoX with QMIX-based algorithms, we present hyperparameters commonly appearing in the baseline algorithms and FoX in Table 3. In addition to describing the hyperparameters presented in FoX in Table 4, we also introduce the structure of the networks proposed in FOX.

Event	Checkpoint reward	Score reward
Our team scores	-	+1
Opposing team scores	-	-1
Score from checkpoint	+0.1 · checkpoints	-

Table 2: The reward setting for GRF environment.

E.1 Shared Hyperparameters of the Experiment

FoX is implemented on QMIX (Rashid et al. 2018) with its default hyperparameters suggested by the original paper. QMIX is optimized with the RMSprop optimizer with a learning rate of 5×10^{-4} . Each agent network consists of a fully connected layer followed by a GRU layer with a hidden state of 64 dimensions. The value of ϵ for ϵ -greedy exploration starts at 1.0 and anneals to 0.05 within 50,000 timesteps. The mixing network is composed of 32 dimensions, and we update our target network for every 200 episodes using the recent 5000 episodes from the buffer. Each algorithm was tested for 4 random seeds on SMAC, and 5 random seeds on GRF. Table 3 describes the common parameters used in our experiments.

Parameters	FoX	CDS	EMC	MASER	QMIX	ROMA	MAVEN	LIIR	COMA
Optimizer	RMSProp	RMSProp	RMSProp	RMSProp	RMSProp	RMSProp	RMSProp	RMSProp	RMSProp
Agent Runner	Episode	Episode	Episode	Episode	Episode	Parallel	Episode	Parallel	Parallel
ϵ anneal step	50000	50000	50000	50000	50000	50	50000	50000	100000
Replay buffer size	5000	5000	5000	5000	5000	5000	5000	32	8
Target update interval	200	200	200	200	200	200	200	200	200
Mini-batch size	32	32	32	32	32	32	32	32	8
Mixing network dimension	32	32	32	32	32	32	32	-	-
Discount factor γ	0.99	0.99	0.99	0.99	0.99	0.99	0.99	0.99	0.99
Learning rate	0.0005	0.0005	0.0005	0.0005	0.0005	0.0005	0.0005	0.0005	0.0005
λ_{reg}	0.1	0.1	-	-	-	-	-	-	-

Table 3: Values for hyperparameters used in the experiment.

E.2 Implementation Details of FoX

\mathcal{F} -Net consists of an encoder and two decoders where each structure consists of two fully-connected layers followed by the output layer. With a hidden state of 128 dimensions, the Adam optimizer was used with a learning rate of 1×10^{-3} , trained on 25 samples per iteration. The agent network, divided into individual Q-functions $Q^{Loc,i}$, shared Q-function Q^{Shared} , and formation-based Q-function $Q^{\mathcal{F}}$, shares an identical structure with the agent networks from QMIX, with a fully connected layer followed by a GRU layer with a hidden state of 64 dimensions.

The hyperparameters introduced by FoX includes: β_1 controlling r^{exp} , β_2 the r^{aware} , l the binning capacity of $round()$ function (detailed explanation is provided in section A), m the length of hashcode, and λ_{GF} the gradient flipping. We searched over $\beta_1 \in \{0.001, 0.005, 0.01, 0.02, 0.1\}$, $\beta_2 \in \{0.001, 0.005, 0.01, 0.05\}$, and $l \in \{0, 1, 3\}$. Whereas λ_{GF} for gradient flipping and m for the length of hash code was set to $\lambda_{GF} = 0.1$ and $m = 9$ in all experiments with the exception of the modified 2s3z. The experimental results reported in the paper were conducted using the parameters listed in Table 4.

Environment	β_1	β_2	l	m	λ_{GF}
Starcraft Multi-agent Challenge (Sparse)					
2m_vs_1z (Sparse)	0.1	0.01	3	9	0.1
3m (Sparse)	0.02	0.02	1	9	0.1
2s3z (Sparse)	0.01	0.01	3	9	0.1
8m (Sparse)	0.02	0.02	1	9	0.1
Google Research Football					
Academy_3_vs_1_with_keeper	0.01	0.01	3	9	0.1
Academy_counterattack_hard	0.01	0.01	3	9	0.1
Academy_corner	0.01	0.01	3	9	0.1

Table 4: Best hyperparameter setup.

Compared to other scenarios, in the 2m_vs_1z environment, comparably higher value of $\beta_1 = 0.1$ demonstrated optimal

performance. This is attributed to the characteristic of the environment where positive rewards can be obtained only once per episode. In such a scenario, increasing the effect of exploration through higher β_1 values appeared to be advantageous. Whereas, in GRF, $\beta_1 = 0.01$ and $\beta_2 = 0.01$ generally showed the best performance.

F Exploration path on GRF

Figure 9 illustrates the exploration path of FoX as the agent becomes aware of its current formation. During initialization ($t = 0$), formations are formulated outside of the agents' sight range. Due to partial observability, these formations are not well-awareable for agents. Consequently, agents are encouraged to explore formations that they can be better aware of. At $t = 10$ and $t = 20$, we can still see that the agents are exploring for formations they can be aware of. Starting from $t = 30$, as the agents finally achieve a formation that they can be aware of, the amount of exploration decreases, and agents start to focus on maximizing r^{ext} , the reward from the environment.

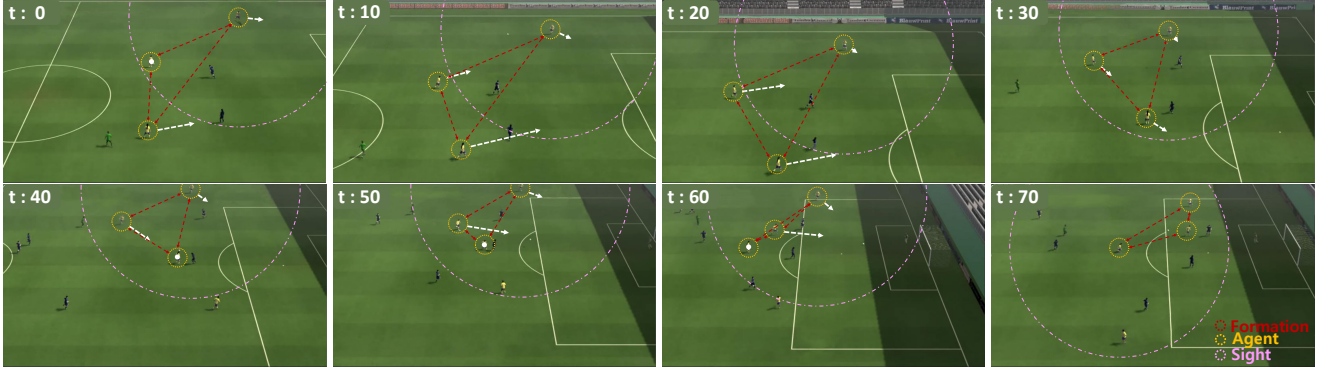


Figure 9: Exploration path on GRF *Academy_counterattack_hard*

G Intrinsic Reward Analysis

In this section, we evaluate how the intrinsic rewards r^{exp} and r^{aware} behave as learning progresses. According to Figure 10, the agents are unable to formulate a winning strategy initially ($t = 0$), so the agents are led to visit various formations. However, we actually observe a decrease in r^{exp} due to the repeated occurrences of states where all ally agents are eliminated. At $t = 0.5M$, we can observe r^{exp} starts to increase. But at this point in time, we still observe a decrease in the r^{aware} as the agents explore diverse formations. Finally, at $t = 2.5M$, where the agents have successfully learned strategies to win the combat, we can observe both r^{exp} and r^{aware} fastly approaching zero, as it is optimal to maximize the r^{ext} from the environment.

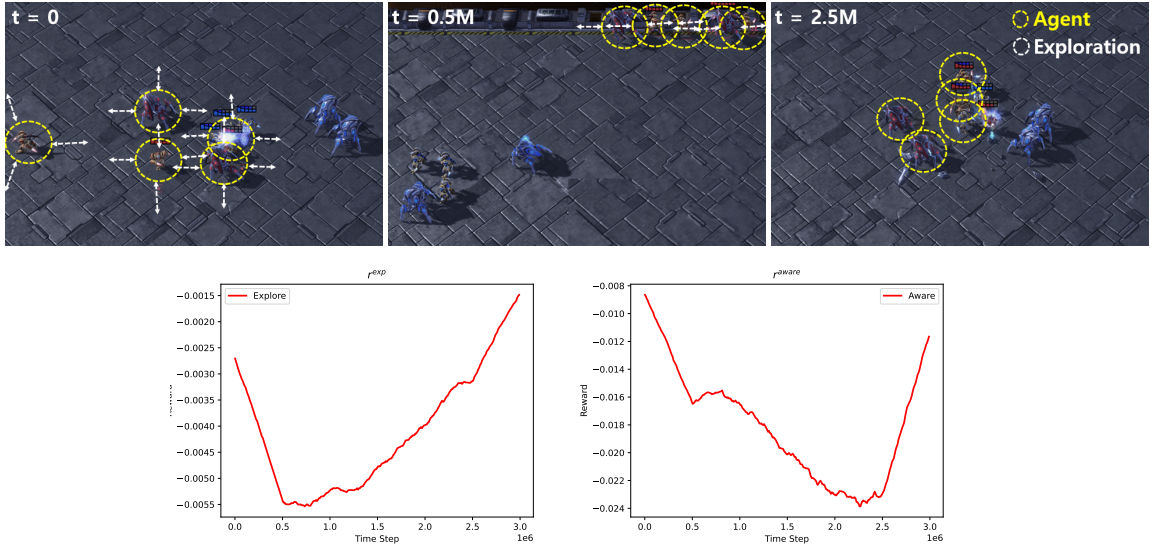


Figure 10: Agent behaviors according to intrinsic rewards